


RESEARCH ARTICLE



## Bazi Bushen capsule attenuates cognitive deficits by inhibiting microglia activation and cellular senescence

Chuanyuan Ji<sup>a,b</sup>, Cong Wei<sup>b,c</sup>, Mengnan Li<sup>b,c</sup>, Shuang Shen<sup>a</sup>, Shixiong Zhang<sup>a,b</sup>, Yunlong Hou<sup>b,c</sup>  and Yiling Wu<sup>a,b</sup>

<sup>a</sup>School of Traditional Chinese Medicine & School of Integrated Traditional Chinese and Western Medicine, Nanjing University of Chinese Medicine, Nanjing, China; <sup>b</sup>National Key Laboratory of Collateral Disease Research and Innovative Chinese Medicine, Shijiazhuang, China; <sup>c</sup>Key Laboratory of State Administration of TCM (Cardio-Cerebral Vessel Collateral Diseases), Shijiazhuang, China

### ABSTRACT

**Context:** Bazi Bushen capsule (BZBS) has anti-ageing properties and is effective in enhancing memory.

**Objective:** To find evidence supporting the mechanisms and biomarkers by which BZBS functions.

**Materials and methods:** Male C57BL/6J mice were randomly divided into five groups: normal, ageing,  $\beta$ -nicotinamide mononucleotide capsule (NMN), BZBS low-dose (LD-BZ) and BZBS high-dose (HD-BZ). The last four groups were subcutaneously injected with D-galactose (D-gal, 100 mg/kg/d) to induce the ageing process. At the same time, the LD-BZ, HD-BZ and NMN groups were intragastrically injected with BZBS (1 and 2 g/kg/d) and NMN (100 mg/kg/d) for treatment, respectively. After 60 days, the changes in overall ageing status, brain neuron morphology, expression of p16<sup>INK4a</sup>, proliferating cell nuclear antigen (PCNA), ionized calcium-binding adapter molecule 1 (Iba1), postsynaptic density protein 95 (PSD95), CD11b, Arg1, CD206, Trem2, Ym1 and Fizz1, and the senescence-associated secretory phenotype (SASP) factors were observed.

**Results:** Compared with the mice in the ageing group, the HD-BZ mice exhibited obvious improvements in strength, endurance, motor coordination, cognitive function and neuron injury. The results showed a decrease in p16<sup>INK4a</sup>, Iba1 and the upregulation of PCNA, PSD95 among brain proteins. The brain mRNA exhibited downregulation of Iba1 ( $p < 0.001$ ), CD11b ( $p < 0.001$ ), and upregulation of Arg1 ( $p < 0.01$ ), CD206 ( $p < 0.05$ ), Trem2 ( $p < 0.001$ ), Ym1 ( $p < 0.01$ ), Fizz1 ( $p < 0.05$ ) and PSD95 ( $p < 0.01$ ), as well as improvement of SASP factors.

**Conclusions:** BZBS improves cognitive deficits via inhibition of cellular senescence and microglia activation. This study provides experimental evidence for the wide application of BZBS in clinical practice for cognitive deficits.

### ARTICLE HISTORY

Received 12 April 2022  
Revised 16 August 2022  
Accepted 27 September 2022

### KEYWORDS

Synaptic plasticity; microglia polarization; senescence-associated secretory phenotype; ageing; traditional Chinese medicine


## Introduction

The process of ageing involves progressive degradation of physiological functions, leading to increased morbidity and mortality. Brain function gradually declines during the ageing process, which manifests as impairments in memory, learning, exploration, coordination and motor abilities (Alexander et al. 2012; Levin et al. 2014). These phenomena increase the aged brain's susceptibility to Alzheimer's disease (AD), stroke and Parkinson's disease (Mattson and Arumugam 2018).

Targeting the mechanisms of ageing has been shown to affect age-related cognitive deficits. Cellular senescence and inflammation can be considered signs of ageing and may also play pivotal roles in brain ageing (Mattson and Arumugam 2018; Saez-Atienzar and Masliah 2020). APP/PS1 mice treated with the NAD<sup>+</sup> precursor nicotinamide riboside for over 5 months exhibited increased brain levels of NAD<sup>+</sup>, downregulation of pro-inflammatory factors, decreased cellular senescence, and the activation of microglia in the AD-afflicted brains (Hou et al. 2021).

Notably, several small molecules originating from herbal medicines have been proven to be effective in delaying ageing and exert protective effects on neurodegenerative diseases (Tewari et al. 2018; Kim and Kim 2019; Cui et al. 2020; Ahmad et al. 2021). Intermittent treatment of APP/PS1 mice with the FDA-approved combination of dasatinib and quercetin was found to selectively clear senescent oligodendrocyte progenitor cells and to ameliorate both cognitive impairments and A $\beta$  plaque-associated inflammation (Zhang et al. 2019). Quercetin is designated as a senolytic due to its ability to prolong healthy lifespan and reduce the likelihood of developing age-related diseases by selectively killing senescent cells (Zhu et al. 2015). More recently, fisetin has been identified as a new senolytic that is capable of protecting neurons and improving cognitive function via anti-inflammatory processes, promotion of synaptic plasticity, and elimination of cellular senescence (Singh et al. 2018; Yousefzadeh et al. 2018).

The pathogenesis of neurodegenerative diseases is complex and involves various molecular mechanisms. Thus, the treatment of neurodegenerative diseases should be aimed at multiple potential molecular targets. Accordingly, Chinese herbal medicines and

**CONTACT** Yiling Wu  [professorylw@163.com](mailto:professorylw@163.com); Yunlong Hou  [hoyunlonghrb@hotmail.com](mailto:hoyunlonghrb@hotmail.com)  National Key Laboratory of Collateral Disease Research and Innovative Chinese Medicine, Shijiazhuang, China

© 2022 The Author(s). Published by Informa UK Limited, trading as Taylor & Francis Group.

This is an Open Access article distributed under the terms of the Creative Commons Attribution-NonCommercial License (<http://creativecommons.org/licenses/by-nc/4.0/>), which permits unrestricted non-commercial use, distribution, and reproduction in any medium, provided the original work is properly cited.

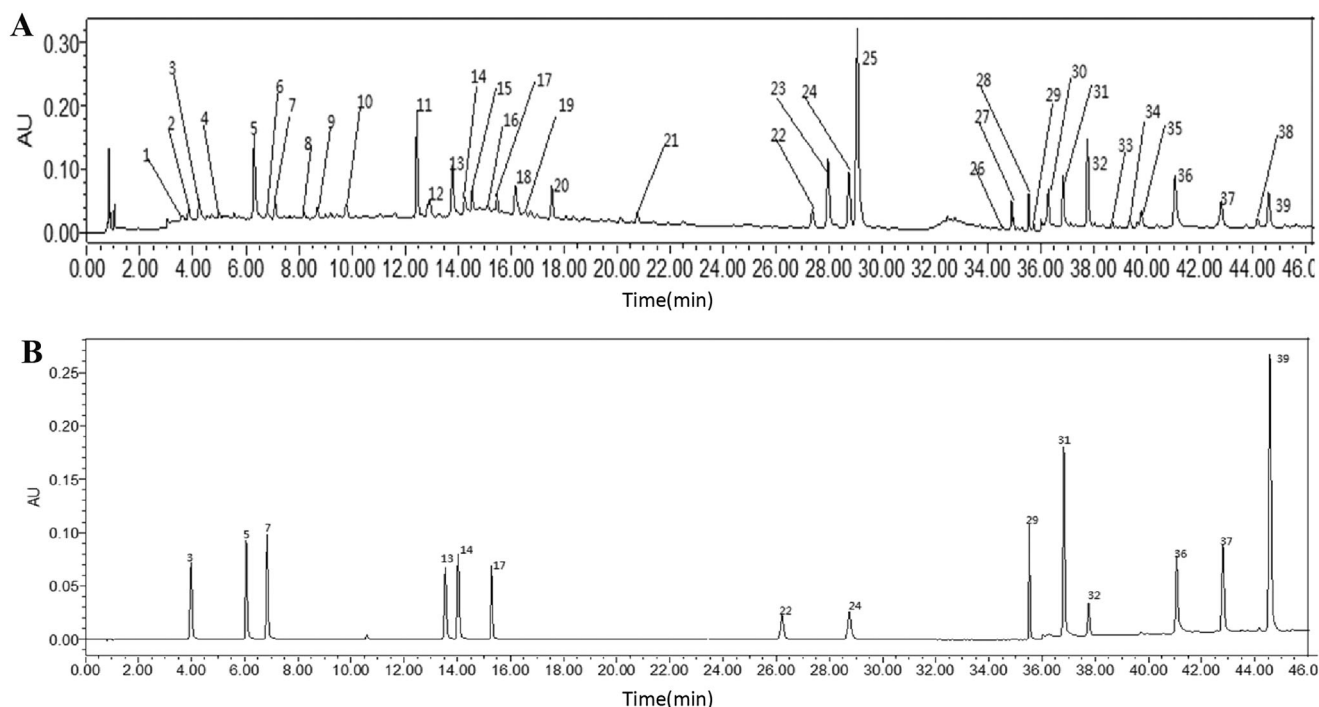


**Figure 1.** UPLC of BZBS (A) and reference substance (B) mixed reference substance. Compound 3: neochlorogenic acid; compound 5: chlorogenic acid; compound 7: cryptochlorogenic acid; compound 13: isoquercitrin; compound 14: hyperoside; compound 17: verbascoside; compound 22: epimedin A; compound 24: icariin; compound 29: baohuoside I; compound 31: imperatorin; compound 32: osthole; compound 36: catalpol; compound 37: deoxyschizandrin; compound 39: schisandrin B.

extracts can act on diverse molecular targets in an additive manner or even synergistically and are increasingly used to treat neurodegenerative diseases (Long et al. 2015; Tewari et al. 2018). Bazi Bushen capsule (BZBS) comprises 16 Chinese medicines (Huang et al. 2021) and is highly effective at relieving fatigue, curing impotence and male infertility, tonifying the kidneys, and delaying the ageing process in clinical studies (Huang et al. 2021; Li et al. 2021).

Chemical analysis has identified 14 unique substances in BZBS by ultra-performance liquid chromatography/mass spectrometry (UPLC/MS) (Huang et al. 2021; Figure 1, Table 1). These include chlorogenic acids, flavonoids, phenylethanoid glycosides, coumarins, lignans and terpenoid catalpol, which contain a variety of anti-ageing natural plant components and protect against age-related cognitive deficits (Wei et al. 2018; Yan et al. 2018; Zhang et al. 2019; Wang C et al. 2020; Fernandes et al. 2021; Wang YL et al. 2021). Recent studies indicate that BZBS is effective at regulating lipid metabolism (Huang et al. 2020) and treating post-menopausal atherosclerosis in ovariectomized female *Ovx/ApoE<sup>-/-</sup>* mice (Huang et al. 2021).

Moreover, BZBS can improve the degeneration of testicular morphology and spermatogenesis by regulating the Sirt6/NF- $\kappa$ B and Sirt6/P53 pathways in ageing mice induced by D-galactose (D-gal) and NaNO<sub>2</sub> (Li et al. 2021). Additionally, BZBS is effective at ameliorating brain function decline in D-gal- and NaNO<sub>2</sub>-induced ageing mice, which may be associated with protecting redox homeostasis, telomere integrity, apoptosis inhibition, and activation of the Sirt6/P53-PGC-1 $\alpha$ -TERT and Sirt6/NRF2/HO-1 signalling pathway (Li et al. 2022). Currently, the mechanism of BZBS delaying ageing and improving brain ageing still needs further research. Furthermore, it remains to be resolved whether BZBS prevents and treats brain ageing by inhibiting cellular senescence and neuroinflammation, which are two key factors that lead to ageing.

In this study, the effects and mechanism of BZBS regarding age-related cognitive deficits were investigated with D-gal-induced ageing in a mouse model. The results show that BZBS is effective

at attenuating neuron injury and the decline of synaptic density and plasticity, thereby preventing age-related cognitive decline. These effects may be related to the inhibition of neuroinflammation and cellular senescence by BZBS.

## Materials and methods

### Drugs and chemicals

BZBS (Lot: B2006011, Shijiazhuang, China) and  $\beta$ -nicotinamide mononucleotide capsules (NMN, Lot: T19L075, Shijiazhuang, China) were provided by Shijiazhuang Yiling Pharmaceutical Co. Ltd. (Shijiazhuang, China). BZBS and NMN were suspended in 0.5% sodium carboxymethylcellulose (CMC-Na) separately and administered to mice with intragastric (i.g.) injection. D-Gal was purchased from Sigma-Aldrich (St. Louis, MO) and dissolved in sterilized injection water (SIW) filtered through a 0.22  $\mu$ m microporous membrane (PALL, PR, Port Washington, NY). Each mouse received a subcutaneous (s.c.) injection on the back of the neck with D-gal once per day.

### Experiments and sample preparation

Seventy C57BL/6J male mice (8 weeks old, 18–22 g) were procured from Beijing Vital River Laboratory Animal Technology Co. Ltd. (Beijing, China). Five mice were housed in each cage and maintained at 20–26 °C with 40–70% humidity, a 12 h light/dark cycle, and *ad libitum* access to water and food. The Ethics Commission of the Hebei Yiling Chinese Medicine Research Institute approved this study (no. N2020101).

After acclimation for 30 days, the mice were randomly divided into following five groups: normal, ageing, NMN (100 mg/kg/d), BZBS low-dose group (LD-BZ, 1 g/kg/d) and BZBS high-dose group (HD-BZ, 2 g/kg/d). Mice in the last four groups ( $n = 15$  mice per group) were s.c. injected with D-gal (100 mg/kg/d)

**Table 1.** Precision test of relative area.

Peak	RT (time)	Relative area					Mean	SD	RSD%
		Test 1	Test 2	Test 3	Test 4	Test 5			
1	3.52	0.0590	0.0589	0.0588	0.0587	0.0594	0.0590	0.0003	0.4716
2	3.72	0.1316	0.1322	0.1289	0.1324	0.1331	0.1316	0.0016	1.2267
3 <sup>a</sup>	4.15	0.2493	0.2445	0.2389	0.2418	0.2471	0.2443	0.0041	1.6967
4	4.93	0.0583	0.0595	0.0588	0.0595	0.0591	0.0590	0.0005	0.8605
5 <sup>a</sup>	6.30	1.0000	1.0000	1.0000	1.0000	1.0000	1.0000	0.0000	0.0000
6	6.80	0.0306	0.0310	0.0299	0.0307	0.0301	0.0305	0.0005	1.4806
7 <sup>a</sup>	7.12	0.1947	0.1929	0.1986	0.1910	0.1974	0.1949	0.0031	1.6146
8	8.24	0.0635	0.0613	0.0615	0.0612	0.0611	0.0617	0.0010	1.6371
9	8.74	0.1242	0.1237	0.1234	0.1246	0.1240	0.1240	0.0005	0.3655
10	9.88	0.1835	0.1867	0.1797	0.1832	0.1822	0.1831	0.0025	1.3749
11	12.67	0.9813	0.9592	0.9752	0.9765	0.9762	0.9737	0.0084	0.8671
12	13.16	0.4325	0.4253	0.4293	0.4236	0.4184	0.4258	0.0054	1.2715
13 <sup>a</sup>	14.02	0.7183	0.7224	0.7152	0.7227	0.7261	0.7209	0.0042	0.5857
14 <sup>a</sup>	14.47	0.1715	0.1682	0.1753	0.1685	0.1692	0.1706	0.0030	1.7392
15	14.73	0.1499	0.1498	0.1504	0.1482	0.1511	0.1499	0.0011	0.7220
16	15.33	0.0661	0.0654	0.0660	0.0662	0.0661	0.0659	0.0003	0.4972
17 <sup>a</sup>	15.71	0.1596	0.1605	0.1599	0.1605	0.1607	0.1602	0.0005	0.2868
18	16.43	0.4899	0.4970	0.4851	0.4899	0.4821	0.4888	0.0056	1.1549
19	16.82	0.0613	0.0616	0.0618	0.0622	0.0618	0.0617	0.0003	0.5588
20	17.85	0.4007	0.3992	0.3851	0.3909	0.3977	0.3947	0.0066	1.6605
21	21.20	0.1570	0.1560	0.1618	0.1555	0.1579	0.1576	0.0025	1.6022
22 <sup>a</sup>	27.92	0.2556	0.2513	0.2536	0.2508	0.2596	0.2542	0.0036	1.4242
23	28.52	0.9500	0.9476	0.9557	0.9367	0.9503	0.9481	0.0070	0.7374
24 <sup>a</sup>	29.31	0.5813	0.5632	0.5579	0.5549	0.5572	0.5629	0.0107	1.9076
25	29.64	2.8239	2.7121	2.7489	2.8284	2.8226	2.7872	0.0534	1.9158
26	34.71	0.0231	0.0239	0.0236	0.0232	0.0232	0.0234	0.0003	1.3942
27	35.07	0.2471	0.2564	0.2490	0.2481	0.2482	0.2498	0.0038	1.5093
28	35.71	0.1936	0.1967	0.1976	0.1956	0.1961	0.1959	0.0015	0.7701
29 <sup>a</sup>	35.93	0.0539	0.0538	0.0536	0.0546	0.0529	0.0538	0.0006	1.1037
30	36.50	0.3576	0.3532	0.3639	0.3644	0.3621	0.3603	0.0048	1.3201
31 <sup>a</sup>	37.09	0.4611	0.4617	0.4709	0.4676	0.4662	0.4655	0.0041	0.8860
32 <sup>a</sup>	38.05	0.9762	0.9760	0.9609	0.9704	0.9841	0.9735	0.0086	0.8794
33	39.02	0.0609	0.0620	0.0615	0.0614	0.0621	0.0616	0.0005	0.8024
34	39.71	0.0968	0.0943	0.0965	0.0966	0.0972	0.0963	0.0012	1.2086
35	40.17	0.2999	0.3019	0.3053	0.2987	0.2980	0.3008	0.0029	0.9780
36 <sup>a</sup>	41.49	0.5160	0.5185	0.5067	0.5232	0.5182	0.5165	0.0061	1.1802
37 <sup>a</sup>	43.31	0.3732	0.3747	0.3742	0.3661	0.3809	0.3738	0.0053	1.4101
38	44.75	0.0977	0.0935	0.0954	0.0979	0.0963	0.0962	0.0018	1.8717
39 <sup>a</sup>	45.18	0.3702	0.3830	0.3821	0.3896	0.3829	0.3815	0.0070	1.8418

<sup>a</sup>14 substances. Compound 3: neochlorogenic acid; compound 5: chlorogenic acid; compound 7: cryptochlorogenic acid; compound 13: isoquercitrin; compound 14: hyperoside; compound 17: verbascoside; compound 22: epimedins A; compound 24: icariin; compound 29: baohuoside I; compound 31: imperatorin; compound 32: osthole; compound 36: catalpol; compound 37: deoxyschizandrin; compound 39: schizandrin B.

dissolved in SIW once daily for 60 days to induce a process of ageing. Mice in the normal group ( $n=10$ ) were injected with SIW once per day with an equal volume.

From the first day of modelling, the NMN group was i.g. administered 100 mg/kg/day of a suspension of NMN in 0.5% CMC-Na. The LD-BZ and HD-BZ mice were i.g. administered suspensions of BZSB in 0.5% CMC-Na over a period of 8 weeks at doses of 1 and 2 g/kg/day, respectively. Mice in the normal and ageing groups were administered an equivalent volume of 0.5% CMC-Na. The detailed procedure is shown in Figure 2.

### Appearance and fur

On the second day after the model was established and the therapeutic process completed, the appearance, fur colour and gloss of the mice were observed and photographed.

### Suspension test

A suspension test was first performed to examine the behaviour of the mice. The mice were placed on a hanging net. After they grasped the net firmly, the net was turned over, and the duration until landing was recorded for each mouse.

### Grip test

Next, a grip test was performed. A mouse was placed on a detection net in the same position as in the grip-measuring test (Chatillon, Largo, FL). After the mouse's limbs firmly grasped the net, the mouse's tail was pulled and held parallel to the detection net. This process was repeated three times. A digital force gauge measured the grip strength and displayed the maximum value.

### Rotarod test

A rotarod test was performed by placing the mice on textured drums of IITC Rotarod Treadmills (IITC Inc. Life Science, Woodland Hills, CA). The initial speed of the rotarod was 5 rpm, the maximal speed was 30 rpm, the acceleration time was 30 s, and the test duration was 180 s. The results were recorded when mice dropped onto the individual sensing platforms below. Adaptability training was performed for three consecutive days, and a formal test was performed on the fourth day.

### Barnes maze test

Finally, a Barnes maze test was performed. Before initiating the test, a white background was laid on the ground as a background

## Study Design

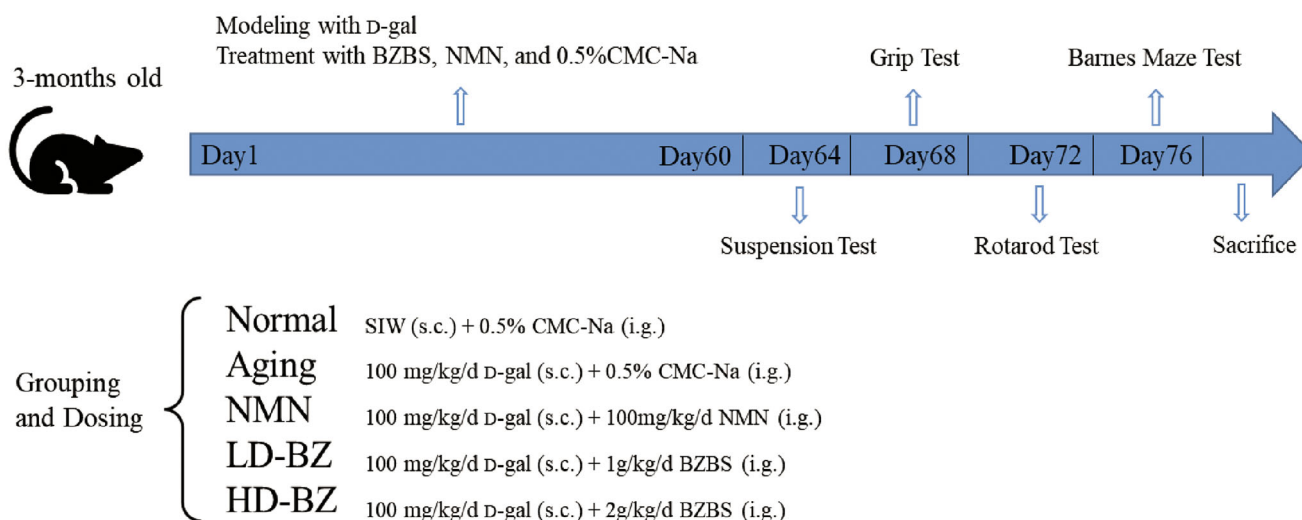


**Figure 2.** The research design of BZBS treatment on ageing mice induced by D-gal.

to help distinguish the mice. Each mouse was placed into a target box to adapt for 3 min (the target box was equipped with steps and dark areas to let the mice escape more easily).

Once training began, the mice were placed under a light-tight box in the centre of a maze to limit their activities for 5 s. The timer began when the light-tight box was removed, and the mice were observed from behind a curtain. An escape was recorded when all four of the mouse's limbs entered the target box. The mouse was left to stay in the box for 30 s.

Each mouse was observed for up to 3 min per time. If the mouse could not locate the target box, it was moved from the maze and placed into the target box for 30 s. Before each test, the maze area was wiped with 75% alcohol to prevent the mouse from relying on smell rather than memory. The mice were trained once each day for three days consecutively and formally tested on the fourth day.

In the formal test, the mouse was restricted in the light-tight box for 5 s, after which the box was removed, and data collection began using a video analysis system for animal behaviour (Jiliang Software Technology, Shanghai, China). The duration of data collection was 3 min, during which the mouse was permitted to move freely. The time threshold was set for 1 s, and the test ceased when the mouse entered the target box and remained for at least 1 s. Each mouse's escape latency to reach the target box and error times (the number of times an error occurred) were recorded. An error was defined as a stretch of the head or exploration of non-target holes.

### Body weight and organ coefficient

The body weights of mice were measured once per week. Mice were sacrificed at the end of all tests, and the organs were weighed using a high-precision electronic balance (Mettler Toledo, Columbus, OH). The organ coefficient was computed using the following equation:

$$\text{organ index g/100 g} = \text{organ weight/body weight} \times 100.$$

### Brain morphology

Brain-tissue sections (4  $\mu\text{m}$ ) were stained with haematoxylin and eosin (H&E) (Solarbio, Beijing, China). After deparaffinizing by

xylene, the sections were rehydrated by alcohol gradients and distilled water. The sections were haematoxylin-stained for 10 min, differentiated by hydrochloric acid alcohol, and rinsed for 15 min using running water. The nucleus was counterstained by eosin for 1 min. Morphological changes were observed, and images were collected by a Nano Zoomer-SQ digital slide scanner (Hamamatsu, Japan).

### Nissl staining

Brain sections (6  $\mu\text{m}$ ) were deparaffinized, rehydrated and treated with toluidine blue solution (Solarbio, Beijing, China) for 30 min at 60  $^{\circ}\text{C}$ . They were then washed in running water and differentiated rapidly in 95% ethanol. Lastly, the sections were dried thoroughly and covered with neutral resin.

### Immunohistochemistry

After deparaffinization, hydration and antigen retrieval, sections were blocked for endogenous peroxidase and non-specific protein binding sites in a wet box containing a small volume of water using an SP kit (a detection system using rabbit streptavidin-biotin) (ZSGB, Beijing, China). Next, we gently removed the liquid from the slices. Primary antibodies were added to the sections and incubated at 4  $^{\circ}\text{C}$  overnight. The primary antibodies were rabbit anti-p16<sup>INK4a</sup> polyclonal antibody (1:200; Abcam, Cambridge, UK) and rabbit anti-proliferating cell nuclear antigen (PCNA) monoclonal antibody (1:500; Abcam, Cambridge, UK).

On the following day, the tissues sections were washed with phosphate-buffered saline (PBS, pH 7.4) three times for 10 min each. Then, biotin-labelled goat anti-rabbit IgG polymer was added to the sections, which were incubated for 15 min and washed with PBS. This was followed by addition of HRP-labelled streptavidin for 15 min. The sections were washed with PBS, stained at room temperature with diaminobenzidine for 3–5 min, counterstained, and covered. Sections were observed and images were collected with a Nano Zoomer-SQ digital slide scanner (Hamamatsu, Japan).

## Immunofluorescence

After deparaffinization, sections were rehydrated and incubated with 0.01 M sodium citrate antigen retrieval buffer (pH 6.0) for antigen retrieval. They were then blocked for non-specific protein and endogenous Fc fragment binding sites using 10% donkey serum in a wet box for 1 h. Next, primary antibodies were added to sections, which were then incubated overnight at 4 °C. The primary antibodies were rabbit anti-postsynaptic density protein 95 (PSD95) polyclonal antibody (1:400; Abcam, Cambridge, UK) and rabbit anti-ionized calcium-binding adapter molecule 1 (Iba1) monoclonal antibody (1:500; Abcam, Cambridge, UK).

After incubation, the sections were washed with PBS three times (10 min/wash) in a shaker and kept with donkey anti-rabbit IgG antibody (1:500; Abcam, Cambridge, UK, red fluorescence) at 37 °C for 1 h away from light exposure. Sections were incubated with DIPA after washing at room temperature for 1 h away from light exposure. A ZEISS laser scanning confocal microscope (Zena, Dogern, Germany) was used to analyse the sections.

## Western blot

The proteins were extracted from brain tissues with high-efficiency RIPA tissue/cell lysate and PMSF (Solarbio, Beijing, China). The protein concentrations were estimated with a BCA protein assay kit (Beyotime Biotechnology, Shanghai, China). In each well, 40 µg of protein were loaded and separated by electrophoresis at 120 V in precast 4–20% polyacrylamide gels (GenScript Biotech, Nanjing, China) and transferred to a nitrocellulose membrane (Millipore, Billerica, MA).

After 1 h at 37 °C in a blocking solution (Beyotime Biotechnology, Shanghai, China), monoclonal or polyclonal antibodies were added to the membrane for overnight incubation at 4 °C. Primary antibodies against p16<sup>INK4a</sup>, PCNA, Iba1 and PSD95 were from Abcam (Cambridge, UK). Antibodies against β-actin were from Cell Signaling Technology (1:1000; CST, Danvers, MA). On the next day, goat anti-rabbit IgG antibody (1:5000; Abcam, Cambridge, UK, red fluorescence) was added to the membrane at 37 °C for 1 h away from light. The Odyssey imaging system and image analysis software (LI-COR Biosciences, Lincoln, NE) were used to quantify the amount of target protein by grey scanning using β-actin as an endogenous reference protein (Table 2).

**Table 2.** Primary and secondary antibodies.

	Antibody	Lot. no.	Dilution
Primary antibody	CDKN2A/p16 <sup>INK4a</sup>	ab189034	1:1000
	PCNA	ab92552	1:1000
	Iba1	ab178846	1:800
	PSD95	Ab18258	1:1000
	β-Actin	49705	1:1000
Secondary antibody	Goat anti-rabbit IgG (IRDye 800 CW)	ab216773	1:5000
	Donkey anti-rabbit IgG H&L (Alexa Fluor® 647)	ab150075	1:500

## RNA extraction and qRT-PCR analysis

TRIzol reagent (Invitrogen, Thermo, Waltham, MA) was used for the isolation of total RNA from the brain tissues. NanoDrop One (Thermo, Wilmington, NC) was used for total RNA quantification. RNA was reverse transcribed to cDNA using Perfect Real Time PrimeScript RT Master Mix (Takara Bio, Kusatsu, Japan) on T100 Thermal Cycler PCR amplifier (Bio-Rad Laboratories, Hercules, CA). For quantitative real-time PCR analysis (qRT-PCR), the reaction system used TB Green Premix Ex Taq II (Tli RNase H Plus) (Takara Bio, Kusatsu, Japan) on a LightCycler 96 instrument (Roche, Mannheim, Germany). GAPDH was used as an internal reference gene, and the 2<sup>-ΔΔCt</sup> method was used to determine the expression level of each gene. The sequences of qRT-PCR primers (Sangon Biotech, Shanghai, China) are shown in Table 3.

## Magnetic luminex assay

Brain tissues of mice were lysed with non-denatured tissue/cell lysate (Solarbio, Beijing, China), and brain proteins were quantified with a BCA protein assay kit. The brain and plasma proteins were centrifuged at 16,000×g for 4 min in a multi-purpose, high-speed centrifuge (Gene, Shanghai, China). The proteins were diluted twofold (75 µL proteins of sample + 75 µL of calibration dilution RD6-52) and mixed thoroughly. The diluted proteins were quantified with Mouse Premixed Multi-Analyte kits (LXSAMSM-15, Lot: L137690, R&D, Minneapolis, USA; LXSAMSM-01, Lot: L137689, R&D, Minneapolis, USA, Table 4). This reagent was brought to room temperature before use.

Standards or samples (50 µL each) were added to each well of a microplate, and the diluted microparticle cocktail was resuspended by a vortexer. Diluted microparticle cocktails (50 µL) were added to each well and covered tightly with foil to minimize exposure to light. The microplate was incubated at room temperature for 2 h on a microplate shaker (Wiggins, Straubenhardt, Germany) set at 800 rpm.

The microplate was washed using a magnetic device, which was left to stand for 1 min before the liquid was removed. Each well was filled with 100 µL of wash buffer, which sat for 1 min before being removed. This washing procedure was performed three times, after which 50 µL of diluted biotin-antibody cocktail was added to each well.

We firmly covered and incubated the microplate on a shaker set at 800 rpm for 1 h at room temperature, and the microplate was then washed. To each well, 50 µL of diluted streptavidin-PE solution was added and kept away from light. We firmly covered and incubated the microplate at room temperature on the shaker set at 800 rpm for 30 min and then repeated the washing step. Next, 100 µL of wash buffer was added to each well, and the microparticles were resuspended for 2 min on the shaker set at

**Table 3.** Primer sequences used for gene expression determination.

Primer	Forward	Reverse
Iba1	5'-CGAGCTCATTGGTGGTACT-3'	5'-TTCTCAGAGAGGATGCAGGT-3'
CD11b	5'-CACAAATGGATGGCTTGATGGA-3'	5'-CGTCCACGCAGTCCGGTAA-3'
Arg1	5'-TTTTAGGGTTACGGCCGGTG-3'	5'-CCTCGAGGCTGCTTTTGA-3'
CD206	5'-AGTTGGGTTCTCTGTAGCCAA-3'	5'-ACTACTACTGAGCCACACCTGCT-3'
Trem2	5'-TGGAACCGTCACCATCACTC-3'	5'-TGGTCATCTAGAGGGTCTCC-3'
Ym1	5'-CATTCACTCAGTTATCAGATTCC-3'	5'-AGTGAGTAGCAGCCTTGG-3'
Fizz1	5'-TCCCAGTGAATACTGATGAGA-3'	5'-CCACTCTGGATCTCCCAAGA-3'
Psd95	5'-GTGGGCGGGCAGGATGGTGAA-3'	5'-CCGCCGTTTGTGGGAATGAA-3'
GAPDH	5'-CCTCGTCCCGTAGCAAAATG-3'	5'-TGAGGTCATGAAGGGTCTGT-3'

**Table 4.** Analytes of magnetic Luminex assay.

	Analyte	Dilutions
Inflammatory factors	C-reactive protein/CRP (BR63)	1:2
	IL-1 beta/IL-1F2 (BR19)	1:2
	IL-1 alpha/IL-1F1 (BR47)	1:2
	IL-2 (BR22)	1:2
	IL-6 (BR27)	1:2
	TNF-alpha (BR14)	1:2
	GM-CSF (BR12)	1:2
Chemokines	ICAM-1/CD54 (BR35)	1:2
	CCL3/MIP-1 alpha (BR46)	1:2
	CCL2/JE/MCP-1 (BR18)	1:2
Proteases and regulators	MMP-3 (BR62)	1:2
	MMP9 (BR62)	1:2
	Serpin E1/PAI-1 (BR43)	1:2
Growth factors	IGFBP-3 (BR65)	1:2
	Endoglin/CD105 (BR33)	1:2
Anti-inflammatory factors	IL-10 (BR28)	1:2

800 rpm. We used a Magpix Luminex analyser to read the data within 90 min (Luminex, Austin, TX).

### Statistical analyses

The behavioural test, organ coefficient, gene, protein and senescence-associated secretory phenotype (SASP) factor data were assessed by one-way analysis of variance (ANOVA) or a Kruskal–Wallis *H* (K–WH) test followed by *post hoc* analysis. Values with  $p < 0.05$  were deemed statistically significant.

## Results

### BZBS ameliorates overall functional status in ageing mice

The mice fur from the ageing group was gray and severely depilated (Figure 3(A)). The fur of mice from the LD-BZ and HD-BZ groups was darker, brighter and denser. Before the start of the experiment, the mouse body weights in each group had no obvious difference ( $p > 0.05$ , Figure 3(B)). However, in the final week of dosing, the body weight of mice in the normal, NMN, LD-BZ and HD-BZ groups were higher than in the ageing group ( $p < 0.05$ ). Similarly, the results of organ coefficients showed that the brain, spleen and thymus coefficients decreased in the ageing group compared to the normal group ( $p < 0.01$ ), whereas BZBS treatments increased the organ coefficients relative to the ageing group ( $p < 0.01$ ) (Figure 3(C)). The suspension, grip and rotarod tests showed that endurance, strength and motor coordination were the lowest in the ageing group (Figure 3(D)). Higher strength was observed in the LD-BZ ( $p < 0.05$ ) and HD-BZ ( $p < 0.01$ ) groups than the ageing group. The endurance and motor coordination of the HD-BZ group mice were enhanced significantly relative to the ageing group ( $p < 0.01$ ). Endurance and motor coordination did not differ significantly between the NMN group relative to the ageing group ( $p > 0.05$ ). These results indicate that BZBS treatment improved appearance, body weight, organ coefficients, endurance, strength and motor coordination in ageing mice.

### BZBS improves cognitive deficits and neuronal injury in ageing mice

Brain ageing is one of the earliest signs of ageing and manifests as cognitive impairment. The worst escape latencies and error times in the Barnes maze test were found in the ageing group (Figure 4(A,B)). The escape latency in the LD-BZ ( $p < 0.01$ ) and HD-BZ ( $p < 0.001$ ) groups was shorter than that of the ageing

group. The error times of the HD-BZ group were lower than that of the ageing group ( $p < 0.01$ ). The learning and memory ability of the ageing group declined dramatically, but BZBS treatment ameliorated the cognitive decline in ageing mice.

Neurons are the main components of brain tissue. Nissl bodies are plaque-like or granular substances in neurons and can be used to reflect their function. The hippocampus and cortex are the two most vital brain areas that affect cognition function (Rothschild et al. 2017; Yavas et al. 2019). The results of H&E and Nissl staining showed that Nissl bodies decreased in number and dissolved in the hippocampal dentate gyrus (DG) and cortical areas of the ageing group (Figure 4(C,D)). BZBS treatment ameliorated the decreased number and dissolution of Nissl bodies in hippocampal DG and cortical areas of ageing mice. These results revealed that BZBS improved cognitive deficits and neuronal injury.

### BZBS increases synaptic density and plasticity in brain tissues of ageing mice

Decreased synaptic density and plasticity directly cause cognitive deficits (Varbanov and Dityatev 2017). PSD95 is an essential protein for maintaining postsynaptic membrane receptor activity and stability. Immunofluorescence (IF), Western blot (WB) and qRT-PCR analyses showed that PSD95 expression decreased in hippocampal and cortical regions of the ageing group relative to the normal group ( $p < 0.05$ , Figure 5(A–E)). The HD-BZ group had increased expression of PSD95 in the hippocampal and cortical regions ( $p < 0.01$ ). These results indicate that BZBS preserved the density and plasticity of synapses.

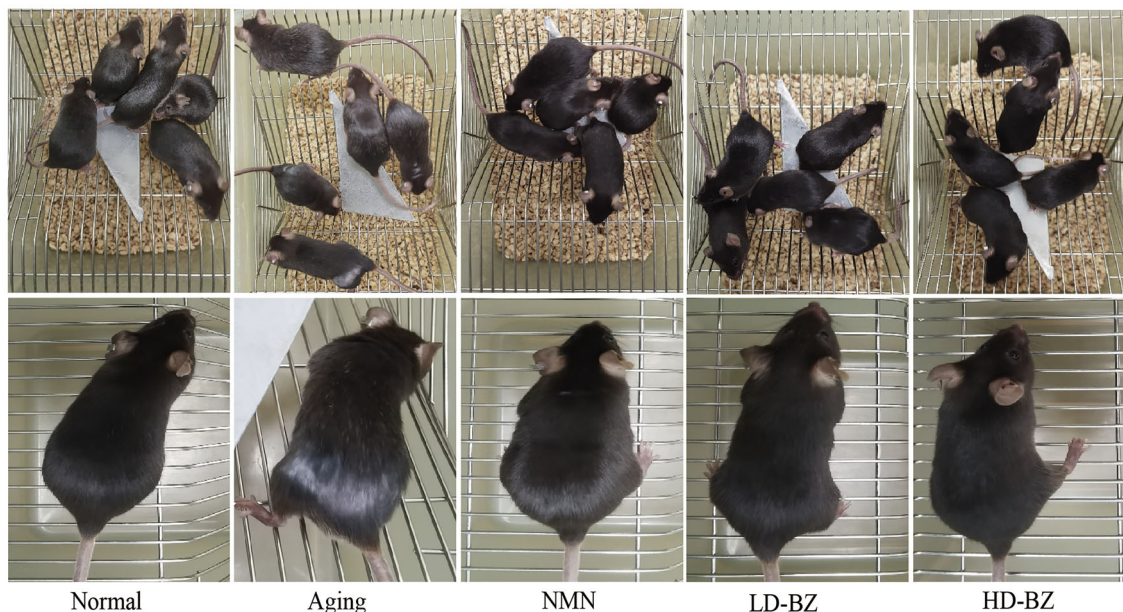
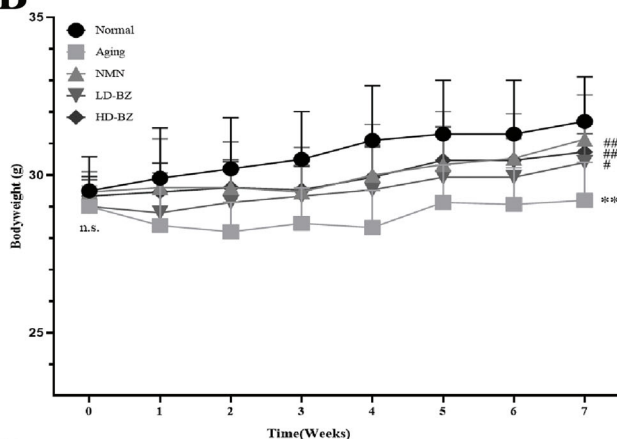
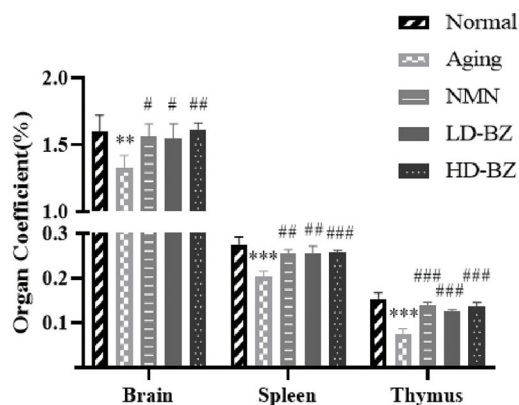
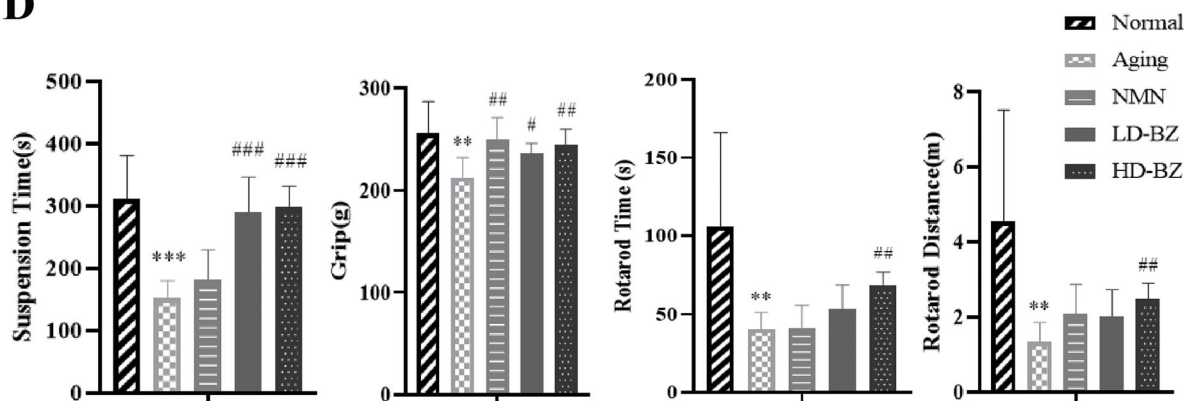
### BZBS inhibits microglia activation and promotes a protective phenotype in brain tissues of ageing mice

Activated microglia in the aged brain increases inflammatory factors that are harmful to synaptic functions (Hou et al. 2021; Zhang et al. 2021). Iba1 is a specific marker of microglia. IF, WB and qRT-PCR analyses showed that the expression of Iba1 increased in hippocampal and cortical regions (Figure 6(A–E)) of the ageing group relative to the normal group ( $p < 0.05$ ). However, BZBS treatment inhibited this increase relative to the ageing group ( $p < 0.01$ ).

Microglia can be classified as protective (M2 phenotype) or detrimental (M1 phenotype), depending on the circumstances (Calsolaro and Edison 2016; Leng and Edison 2021). The qRT-PCR results (Figure 6(E)) indicated that the ageing group's brain tissues had increased mRNA expression of M1 phenotype CD11b and reduced M2 phenotype Arg1, Fizz1, Trem-2, CD206 and Ym1 ( $p < 0.05$ ). Furthermore, the expression of CD11b decreased, and Arg1, Fizz1, Trem-2, CD206 and Ym1 were up-regulated in the HD-BZ group ( $p < 0.05$ ). These results suggest that BZBS inhibited microglia activation. Moreover, microglia in BZBS-treated brains changed into a protective state.

### BZBS alleviates cellular senescence in brain tissues of ageing mice

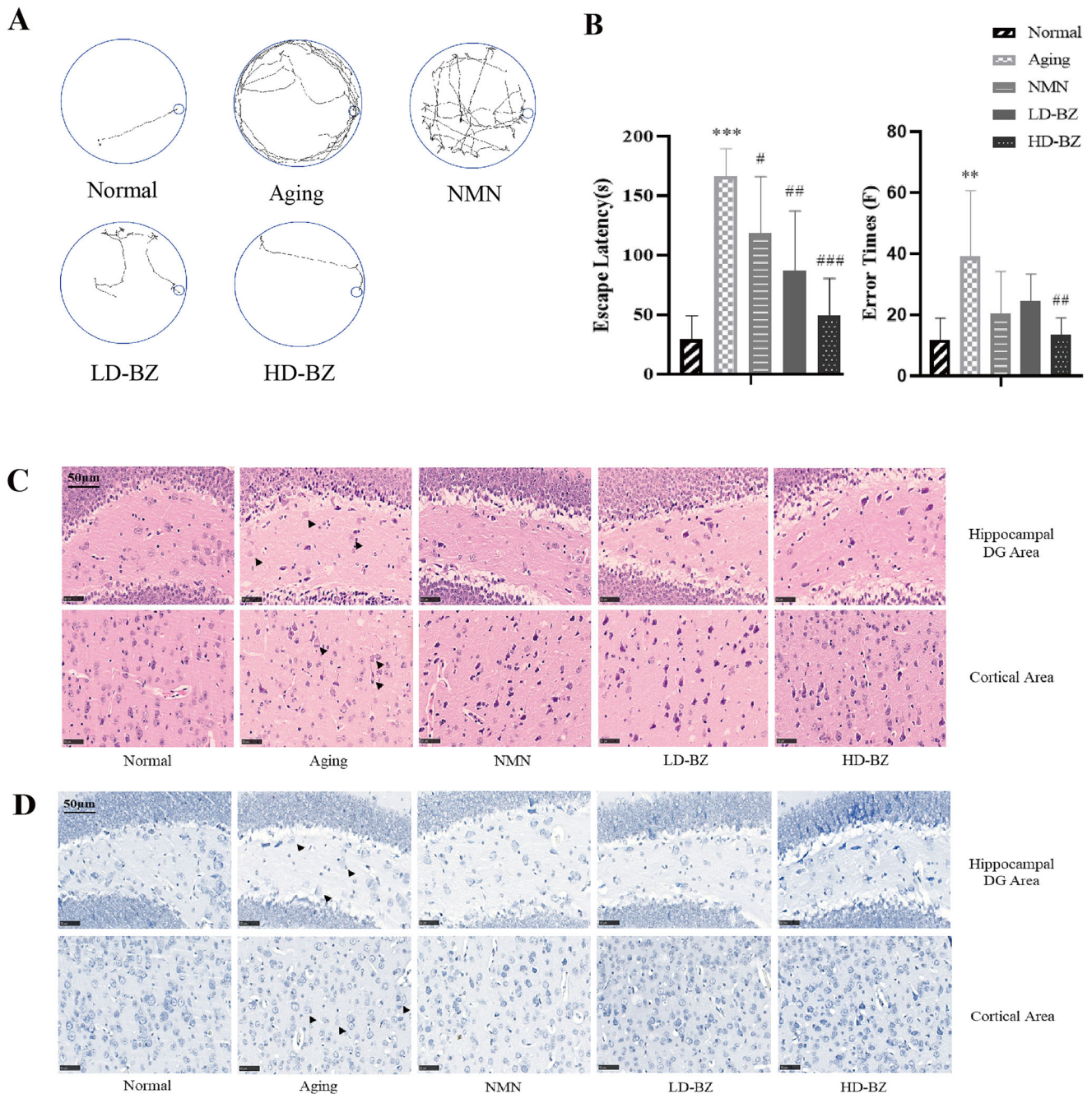
The permanent suspension of cell proliferation is known as cellular senescence (Hayflick 1965; Kuilman et al. 2010). P16<sup>INK4a</sup> is a key factor in cell cycle arrest (Baker et al. 2011, 2016), and PCNA is a gene related to the cell cycle (Lei et al. 2021). Immunohistochemistry (IHC) and WB results indicated that in

**A**

**B**

**C**

**D**


**Figure 3.** The impact of BZBS treatment on age-related behaviours and indicators in  $\alpha$ -gal-induced ageing mice. (A) The appearance of mice. (B) The body weights during administration periods ( $n = 10-15$ ). (C) The brain, spleen and thymus coefficients of mice after administration ( $n = 3$ ). (D) The suspension, grip and rotarod test results of mice ( $n = 7$ ).  $**p < 0.01$  vs. the normal group and  $***p < 0.001$  vs. the normal group;  $\#p < 0.05$  vs. the ageing group,  $\#\#p < 0.01$  vs. the ageing group and  $\#\#\#p < 0.001$  vs. the ageing group.

the ageing group, the expression of  $p16^{INK4a}$  ( $p < 0.05$ ) increased and PCNA ( $p < 0.01$ ) decreased in the hippocampal DG and cortical areas compared with the normal group (Figure 7(A-F)). In the HD-BZ group, the expression of PCNA was higher

( $p < 0.001$ ) and the expression of  $p16^{INK4a}$  was lower ( $p < 0.05$ ) in hippocampal DG and cortical areas than in the ageing group. These results indicated that BZBS inhibited cell proliferation arrest and promoted cell proliferation in the ageing brain.



**Figure 4.** The impact of BZBS treatment on cognitive deficits and neuronal injury in D-gal-induced ageing mice. (A) The Barnes maze test roadmaps of mice. (B) The escape latencies and error times of the Barnes maze tests ( $n = 7$ ). (C) H&E staining images ( $\times 400$ ) of neuron morphology in the hippocampal DG and cortical areas. (D) Toluidine blue staining images ( $\times 400$ ) of Nissl bodies in the hippocampal DG and cortical areas. \*\* $p < 0.01$  vs. the normal group, \*\*\* $p < 0.001$  vs. the normal group; # $p < 0.05$  vs. the ageing group, ## $p < 0.01$  vs. the ageing group and ### $p < 0.001$  vs. the ageing group.

### BZBS inhibits the secretion of SASP factors in plasma and brain tissues of ageing mice

The cell proliferation stagnant state of cell senescence has an inflammatory phenotype, namely SASP, which is manifested by the secretion of pro-inflammatory factors, chemokines, metalloproteinases and growth factors (Coppé et al. 2010; Di Micco et al. 2021). The magnetic Luminex assay of SASP factors in plasma (Figure 8(A)) showed that the level of pro-inflammatory factors IL-1 $\beta$ , IL-1 $\alpha$ , IL-2 and matrix metalloproteinase MMP-9 increased significantly in the ageing group relative to the normal group ( $p < 0.05$ ). The levels of IL-1 $\beta$ , IL-1 $\alpha$  and MMP-9

were lower in the HD-BZ group than the ageing group ( $p < 0.05$ ). The expression of TNF- $\alpha$ , CCL3, IGFBP-3, IL-6, GM-CSF, endoglin, ICAM-1, PAI-1 and CRP increased in the ageing group and decreased following treatment with BZBS. However, the difference was not statistically significant. In addition, the expression of IL-10 significantly decreased in ageing group relative to the normal group ( $p < 0.05$ ), but BZBS treatment significantly increased the expression of IL-10 in plasma ( $p < 0.01$ ).

We also evaluated the expression of SASP factors in brain tissues by magnetic Luminex assay (Figure 8(B)). The expression of IL-1 $\beta$ , ICAM-1, MMP-3 and MMP-9 in the ageing group were



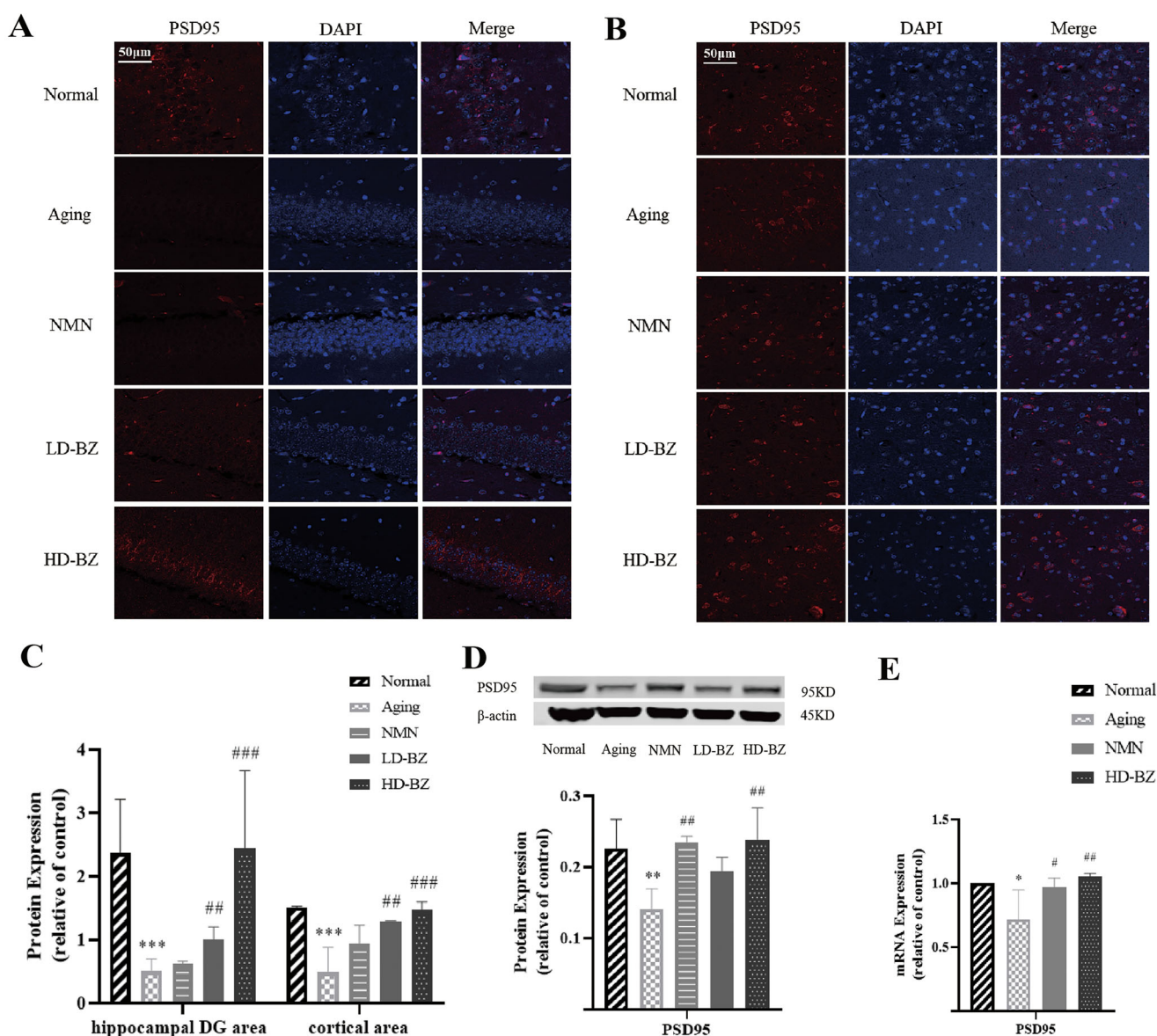


**Figure 5.** The impact of BZBS treatment on synaptic density and plasticity in D-gal-induced ageing mice. (A) IF staining images ( $\times 400$ ) of PSD95 (red) proteins in the hippocampal DG areas. (B) IF staining images ( $\times 400$ ) of PSD95 (red) protein in the cortical areas. (C) Image shows quantification of PSD95 expression in A and B ( $n = 3$ ). (D) WB analysis of PSD95 and  $\beta$ -actin in hippocampal and cortical tissues. Image shows quantification of PSD95, and  $\beta$ -actin was the internal reference protein ( $n = 3$ ). (E) qRT-PCR analysis of PSD95 mRNA levels in hippocampal and cortical tissues, GAPDH gene was used for internal reference ( $n = 3$ ). \* $p < 0.05$  vs. the normal group, \*\* $p < 0.01$  vs. the normal group and \*\*\* $p < 0.001$  vs. the normal group; # $p < 0.05$  vs. the ageing group, ## $p < 0.01$  vs. the ageing group and ### $p < 0.001$  vs. the ageing group.

higher than in the normal group ( $p < 0.05$ ). The levels of ICAM-1, MMP-3 and MMP-9 significantly decreased in brain tissues of the HD-BZ group ( $p < 0.05$ ). The expression of CCL2, CCL3, IL-2, IGFBP-3, PAI-1 and CRP increased in brain tissues of the ageing group and decreased following treatment with BZBS, but the difference was not statistically significant. In other words, BZBS inhibited the SASP factors and upregulated anti-inflammation factors in plasma and brain tissues.

## Discussion

Our results showed that BZBS attenuated cognitive deficits by attenuating the decline of synaptic function and protecting neurons, which may be related to the inhibition of cellular senescence, SASP factor secretion, and the regulation of microglia activation and polarization.

Brain ageing is a significant contributor to neurodegenerative disease development and manifests as cognitive deficits. The ageing model induced by D-gal can simulate the human ageing process and is used extensively to evaluate the pharmacodynamics of drugs aimed at combating ageing and age-related cognitive deficits. This is based on prolonged exposure to D-gal resulting in inflammation in the brain (Sun et al. 2018, 2020; Ahmad et al. 2021), which is a hallmark of brain ageing. Brain ageing in D-gal-induced ageing rodents manifested as fur loss, decreased exercise capacity, and cognitive deficits. In this study, ageing mouse models were successfully established by D-gal. BZBS treatment effectively attenuated cognitive deficits, fur loss, decreased exercise capacity and age-related indicators in D-gal-induced ageing mice relative to the ageing group (Figures 3(A–D) and 4(A,B)).

Neurons are the main components of brain tissue, which exchange information by receiving, integrating, conducting and outputting information. Nissl bodies are plaque-like or granular

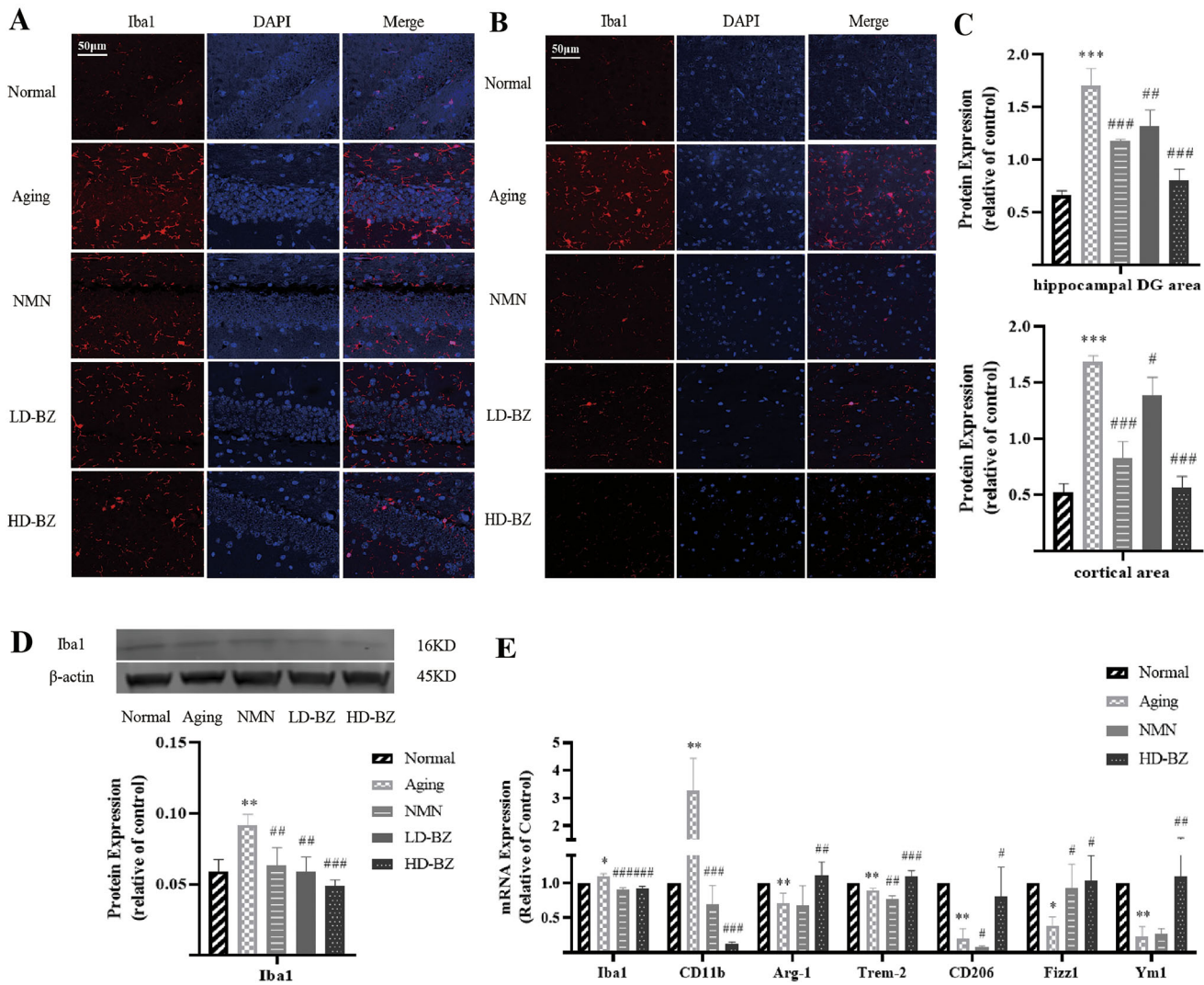


**Figure 6.** The impact of BZBS treatment on activation and polarization of microglia in D-gal-induced ageing mice. (A) IF staining images ( $\times 400$ ) of Iba1 (red) proteins in the hippocampal DG areas. (B) IF staining images ( $\times 400$ ) of Iba1 (red) proteins in the cortical areas. (C) Image shows quantification of Iba1 expression in A and B ( $n=3$ ). (D) WB analysis of Iba1 and  $\beta$ -actin in hippocampal and cortical tissues. Image shows quantification of Iba1, and  $\beta$ -actin was the internal reference protein ( $n=3$ ). (E) qRT-PCR analysis of Iba1, CD11b, Arg-1, Trem-2, CD206, Fizz1 and Ym1 in hippocampal and cortical tissues, GAPDH gene was used for internal reference ( $n=3$ ). \* $p < 0.05$  vs. the normal group, \*\* $p < 0.01$  vs. the normal group and \*\*\* $p < 0.001$  vs. the normal group; # $p < 0.05$  vs. the ageing group, ## $p < 0.01$  vs. the ageing group and ### $p < 0.001$  vs. the ageing group.

substances present in neurons. They are composed of a large number of rough endoplasmic reticulum and free ribosomes, which mainly synthesize proteins required for the renewal of organelles. Nissl bodies can be used as a marker of neuronal functional status. The Nissl bodies undergo decrease, loss and dissolution in an injured neuron. Nissl bodies can increase and return to normal levels in the recovery from neuronal injury (Kaufmann et al. 2012). The current study showed that BZBS can protect against neuronal damage and ameliorate the cognitive deficits in D-gal-induced ageing mice (Figure 4(C,D)).

Synaptic plasticity is the property of being able to adjust the strength of connections between neurons to achieve dynamic changes in signal transmission efficiency (Magee and Grienberger 2020). Impairments in synaptic plasticity and decreased synaptic density are direct causes of cognitive deficits (Varbanov and Dityatev 2017). PSD95 is the most plentiful protein found in the postsynaptic membrane and is essential for maintaining the activity and stability of the receptors on this membrane. In this study, we observed that BZBS ameliorated cognitive deficits by enhancing the density and plasticity of synapses in ageing mice (Figure 5(A-E)).

Neuroinflammation caused by D-gal is the main cause of synaptic plasticity impairments and decreased synapse density (Varbanov and Dityatev 2017). Microglia are one type of innate immune cell in the central nervous system and are the primary and first line of active immune defence (Gao et al. 2016). Under stimulation from injuries, pathogens or pathological stresses, resting state (M0) microglia are activated into a detrimental state (M1) and protective state (M2) in a process called polarization (Zeng et al. 2018). The detrimental microglia generate pro-inflammatory cytokines, including TNF- $\alpha$  and IL-1 $\beta$ , whereas the protective microglia secrete anti-inflammatory cytokines, including IL-10 (Calsolaro and Edison 2016).

In the aged brain, the M1 polarized state is often presented by microglia and characterizes the production of pro-inflammatory factors and amoeboid morphology (Soreq et al. 2017; Mattson and Arumugam 2018). Strategies to reverse or block the phenotypic transition from M2 to M1 in microglia hold immense potential for treating neurodegenerative diseases (Zeng et al. 2018). In this study, BZBS inhibited the increased levels of Iba1 in the hippocampus and cortex of ageing mice induced with

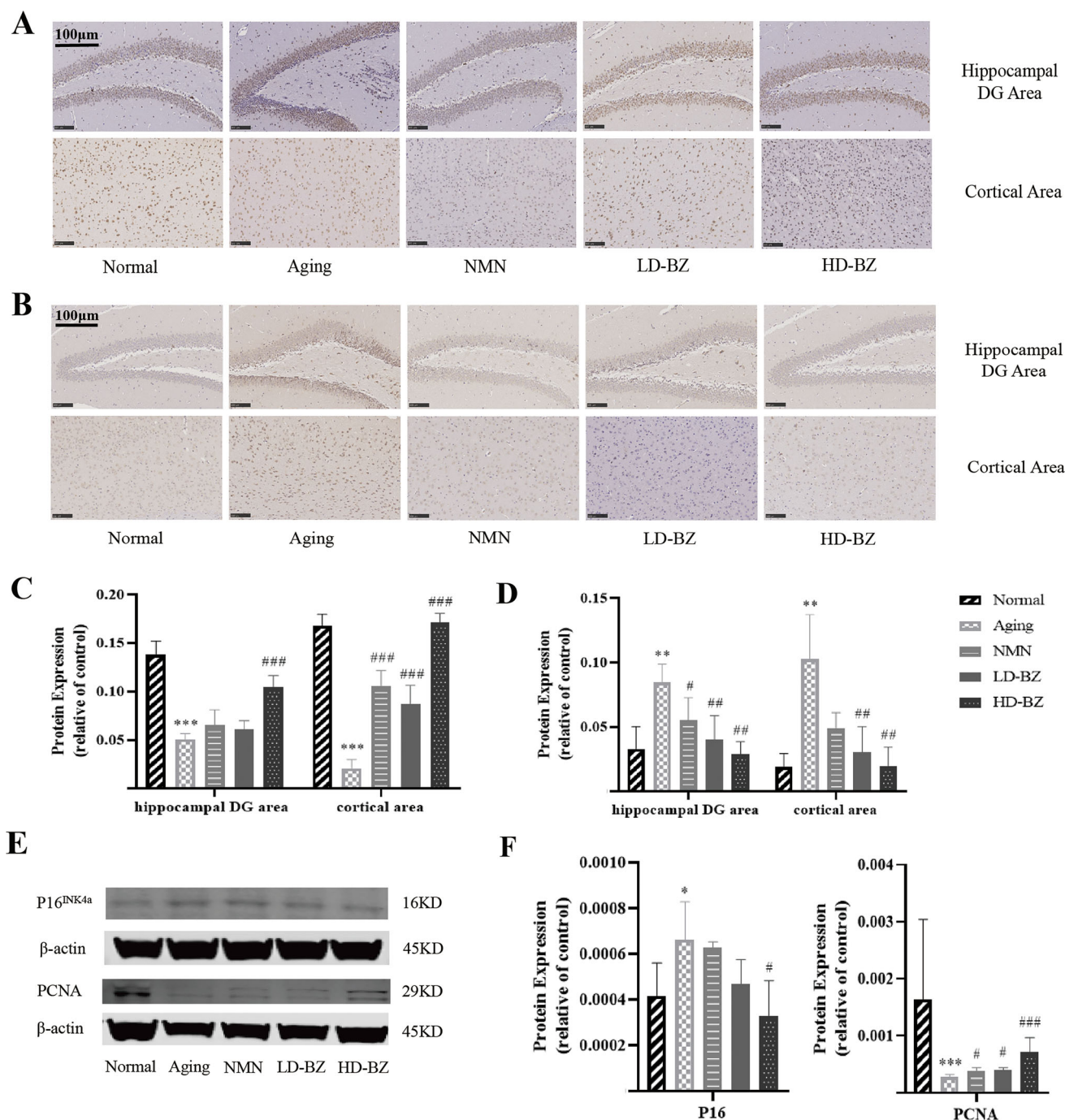


**Figure 7.** The impact of BZBS treatment on the expression of p16<sup>INK4a</sup> and PCNA in D-gal-induced ageing mice. (A) IHC staining images ( $\times 200$ ) of PCNA proteins in hippocampal DG and cortical areas. (B) IHC staining images ( $\times 200$ ) of p16<sup>INK4a</sup> proteins in hippocampal DG and cortical areas. (C) Image shows quantification of PCNA expression in A ( $n = 3$ ). (D) Image shows quantification of p16<sup>INK4a</sup> expression in B ( $n = 3$ ). (E) WB analysis of p16<sup>INK4a</sup>, PCNA and  $\beta$ -actin in hippocampal and cortical tissues. (F) Image shows quantification of p16<sup>INK4a</sup> and PCNA expression in C, and  $\beta$ -actin was the internal reference protein ( $n = 3$ ). \* $p < 0.05$  vs. the normal group, \*\* $p < 0.01$  vs. the normal group and \*\*\* $p < 0.001$  vs. the normal group; # $p < 0.05$  vs. the ageing group, ## $p < 0.01$  vs. the ageing group and ### $p < 0.001$  vs. the ageing group.

D-gal (Figure 6(A–D)). At the transcriptional level, BZBS decreased the levels of detrimental microglia genes and upregulated the levels of protective microglia genes in the hippocampus and cortex regions of ageing mice (Figure 6(E)). Moreover, BZBS treatment significantly enhanced the level of anti-inflammatory factors in the plasma of ageing mice (Figure 8(A)). Therefore, we believe that BZBS inhibited the activation and regulated the polarization of microglia, suggesting that BZBS ameliorated cognitive deficits in ageing mice is associated with exerting anti-neuroinflammation and neuroprotective effects.

The accumulation of senescent cells has become widely accepted as an important factor in cognitive impairment. Some natural compounds derived from herbal medicines, including fisetin, quercetin and curcumin (Lee et al. 2020), have been shown to treat cognitive deficits by eliminating senescent cells. Inflammation is a key factor leading to cellular senescence (Freund et al. 2010; Fielder et al. 2020). Therefore, we hypothesized that cellular senescence is involved in D-gal-induced cognitive deficits in ageing mice characterized by low-grade chronic inflammation.

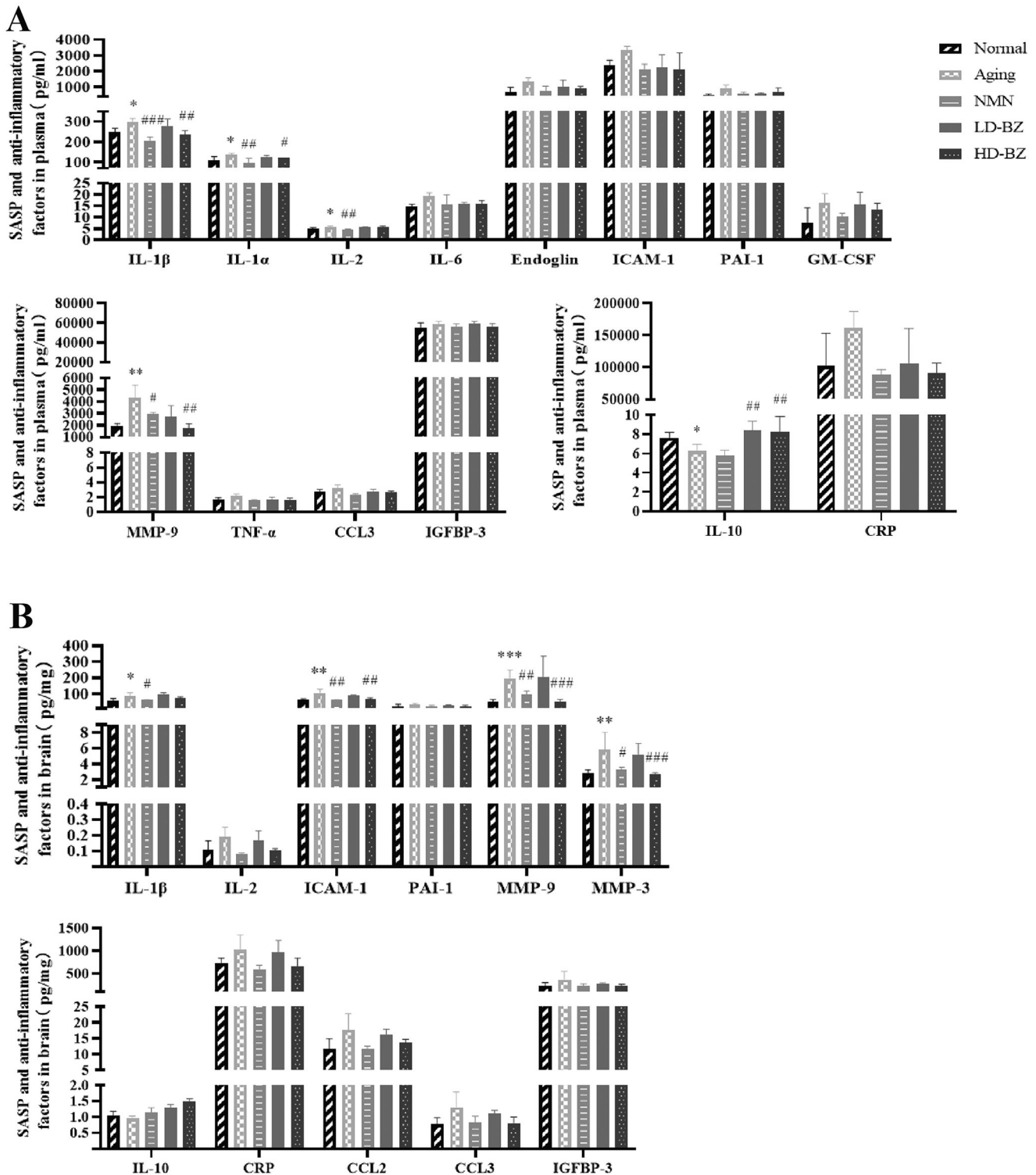


**Figure 8.** The impact of BZBS treatment on SASP and anti-inflammatory factors in D-gal-induced ageing mice. (A) Magnetic Luminex assay for estimating the level of IL-1 $\beta$ , IL-1 $\alpha$ , TNF- $\alpha$ , IL-2, IL-6, ICAM-1, GM-CSF, endoglin, PAI-1, IGFBP3, CCL2, CCL3, MMP-3, MMP-9, CRP and IL-10 in plasma. The expression of CCL-2 and MMP3 was not detected because they exceeded the standard curve range. (B) Magnetic Luminex assay for estimating the level of IL-1 $\beta$ , IL-1 $\alpha$ , TNF- $\alpha$ , IL-2, IL-6, ICAM-1, GM-CSF, endoglin, PAI-1, IGFBP3, CCL2, CCL3, MMP-3, MMP-9, CRP and IL-10 in hippocampal and cortical tissues. \* $p < 0.05$  vs. the normal group, \*\* $p < 0.01$  vs. the normal group and \*\*\* $p < 0.001$  vs. the normal group; # $p < 0.05$  vs. the ageing group, ## $p < 0.01$  vs. the ageing group and ### $p < 0.001$  vs. the ageing group.

Studies have shown that the continual clearance of p16<sup>INK4a</sup>-expressing senescent cells prior to disease onset in an aggressive tauopathy model has a notable effect on gliosis, neurodegeneration and decline in cognition (Bussian et al. 2018). The proliferation of neural precursors declines with age (Miguel-Hidalgo et al. 2014). PCNA is an indispensable marker in maintaining

cell proliferation in actively growing cells (Wang 2014). A homozygous missense sequence alteration of PCNA can cause neurodegeneration and premature ageing. It has been found that the transfer and accumulation of PCNA could rejuvenate stem cells derived from bone marrow of ageing adults (Baple et al. 2014; Lei et al. 2021).

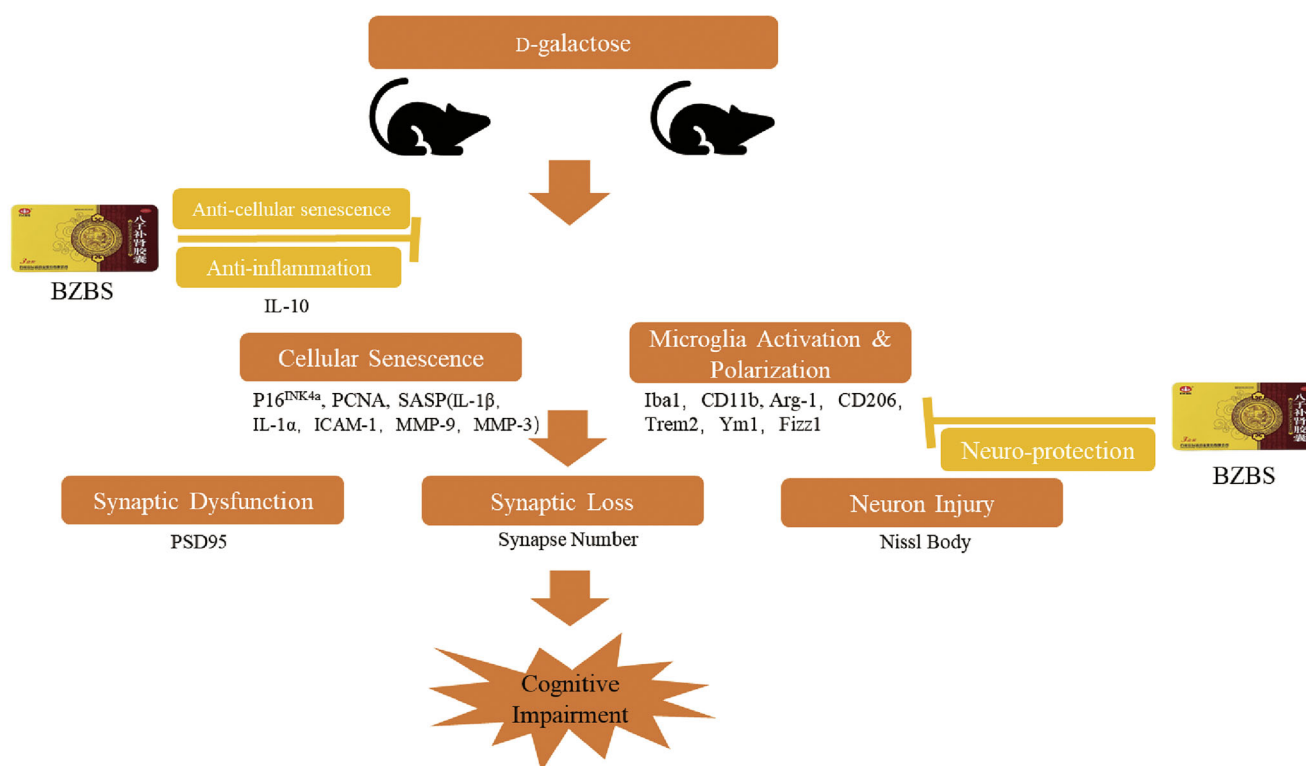


**Figure 9.** The diagram shows that BZBS alleviated cellular senescence and SASP factors secretion, regulated microglia activation and polarization, and transformed activated microglia from a detrimental phenotype to a protective phenotype. BZBS ameliorated neuronal injury, synaptic loss and synaptic dysfunction. BZBS exerted a neuroprotective effect on cognitive deficits.

Senescent cells have SASP, which is a phenomenon exhibiting secretion of pro-inflammatory factors. Prolonged exposure to these factors causes inflammation, which leads to the decline of cognition, synaptic density and plasticity in the aged brain (Guerrero et al. 2021; Jin et al. 2021). Correspondingly, we tested the expression levels of p16<sup>INK4a</sup>, PCNA and SASP factors in D-gal-induced ageing mice. As expected, cellular senescence is involved in cognitive deficit in ageing mice induced with D-gal, and BZBS treatment inhibited the cellular senescence in the hippocampus and cortex regions of ageing mice (Figure 7(A–F)).

Furthermore, ICAM-1, MMP-9 and MMP-3 are overexpressed in neurological diseases and act as pro-inflammatory factors that participate in the development of neuroinflammation (Ringland et al. 2021; Wiera and Mozrzymas 2021; Yang et al. 2021). BZBS treatment decreased the expression of IL-1 $\alpha$ , IL-1 $\beta$  and MMP-9 in plasma and significantly downregulated ICAM-1, MMP-3 and MMP-9 expression in the hippocampus and cortex (Figure 8(A,B)). These results indicated that cellular senescence caused by inflammation led to cognitive deficits in D-gal-induced ageing mice.

BZBS inhibited cellular senescence and neuroinflammation, improved the decline of synapse density and plasticity, and protected neurons, thereby improving cognitive deficits. However, our research has some limitations. First, the component substances of BZBS are not fully known. Second, further research is needed on the potential mechanisms underlying the role of BZBS in improving brain ageing via cellular senescence.

## Conclusions

Our findings suggest that BZBS ameliorates synaptic density and plasticity decline and protected neurons, thus improving cognitive deficits in D-gal-induced ageing mice. These effects may be related

to the inhibition of cellular senescence and regulation of microglia activation and polarization by BZBS (Figure 9). This study provides evidence for the mechanism of action of BZBS in the treatment of age-related cognitive deficits.

## Author contributions

Y.W. and Y.H. conceived the study and assisted with the manuscript; C.J. performed the experiments and wrote the manuscript; C.W., M.L., S.S. and S.Z. assisted with the experiments and analysed the data.

## Disclosure statement

The authors declare that the research was conducted in the absence of any commercial or financial relationships that could be construed as a potential conflict of interest.

## Funding

This work was supported by funding from the National Key Research and Development Program of China (2017YFC1700500); and the Strategic Consulting Project of Chinese Academy of Engineering-Strategic Research on Anti-Aging Effect of Traditional Chinese Medicine (2022-XY-45); and the Natural Science Foundation of Hebei Province (H201906059); and the Scientific Research Project of Hebei Provincial Administration of Traditional Chinese Medicine (2021273).

## ORCID

Yunlong Hou  <http://orcid.org/0000-0002-6989-8221>

## References

- Ahmad S, Khan A, Ali W, Jo MH, Park J, Ikram M, Kim MO. 2021. Fisetin rescues the mice brains against D-galactose-induced oxidative stress, neuroinflammation and memory impairment. *Front Pharmacol.* 12:612078.
- Alexander GE, Ryan L, Bowers D, Foster TC, Bizon JL, Geldmacher DS, Glisky EL. 2012. Characterizing cognitive aging in humans with links to animal models. *Front Aging Neurosci.* 4:21.
- Baker DJ, Childs BG, Durik M, Wijers ME, Sieben CJ, Zhong J, Saltness RA, Jeganathan KB, Verzosa GC, Pezeshki A, et al. 2016. Naturally occurring p16<sup>INK4a</sup>-positive cells shorten healthy lifespan. *Nature.* 530(7589):184–189.
- Baker DJ, Wijshake T, Tchkonina T, LeBrasseur NK, Childs BG, van de Sluis B, Kirkland JL, van Deursen JM. 2011. Clearance of p16<sup>INK4a</sup>-positive senescent cells delays ageing-associated disorders. *Nature.* 479(7372):232–236.
- Baple EL, Chambers H, Cross HE, Fawcett H, Nakazawa Y, Chioza BA, Harlalka GV, Mansour S, Sreekantan-Nair A, Patton MA, et al. 2014. Hypomorphic PCNA mutation underlies a human DNA repair disorder. *J Clin Invest.* 124(7):3137–3146.
- Bussian TJ, Aziz A, Meyer CF, Swenson BL, van Deursen JM, Baker DJ. 2018. Clearance of senescent glial cells prevents tau-dependent pathology and cognitive decline. *Nature.* 562(7728):578–582.
- Calsolaro V, Edison P. 2016. Neuroinflammation in Alzheimer's disease: current evidence and future directions. *Alzheimers Dement.* 12(6):719–732.
- Coppé JP, Desprez PY, Krtolica A, Campisi J. 2010. The senescence-associated secretory phenotype: the dark side of tumor suppression. *Annu Rev Pathol.* 5:99–118.
- Cui X, Lin Q, Liang Y. 2020. Plant-derived antioxidants protect the nervous system from aging by inhibiting oxidative stress. *Front Aging Neurosci.* 12:209.
- Di Micco R, Krizhanovsky V, Baker D, d'Adda di Fagagna F. 2021. Cellular senescence in ageing: from mechanisms to therapeutic opportunities. *Nat Rev Mol Cell Biol.* 22(2):75–95.
- Fernandes MYD, Dobrachinski F, Silva HB, Lopes JP, Gonçalves FQ, Soares FAA, Porciúncula LO, Andrade GM, Cunha RA, Tomé AR. 2021. Neuromodulation and neuroprotective effects of chlorogenic acids in excitatory synapses of mouse hippocampal slices. *Sci Rep.* 11(1):1–11.
- Fielder E, Tweedy C, Wilson C, Oakley F, LeBeau FEN, Passos JF, Mann DA, von Zglinicki T, Jurk D. 2020. Anti-inflammatory treatment rescues memory deficits during aging in *nfk1-/-* mice. *Aging Cell.* 19(10):e13188.
- Freund A, Orjalo AV, Desprez PY, Campisi J. 2010. Inflammatory networks during cellular senescence: causes and consequences. *Trends Mol Med.* 16(5):238–246.
- Gao J, Zhou R, You X, Luo F, He H, Chang X, Zhu L, Ding X, Yan T. 2016. Salidroside suppresses inflammation in a D-galactose-induced rat model of Alzheimer's disease via SIRT1/NF- $\kappa$ B pathway. *Metab Brain Dis.* 31(4):771–778.
- Guerrero A, De Strooper B, Arancibia-Cárcamo IL. 2021. Cellular senescence at the crossroads of inflammation and Alzheimer's disease. *Trends Neurosci.* 44(9):714–727.
- Hayflick L. 1965. The limited in vitro lifetime of human diploid cell strains. *Exp Cell Res.* 37:614–636.
- Hou Y, Wei Y, Lautrup S, Yang B, Wang Y, Cordonnier S, Mattson MP, Croteau DL, Bohr VA. 2021. NAD<sup>+</sup> supplementation reduces neuroinflammation and cell senescence in a transgenic mouse model of Alzheimer's disease via cGAS-STING. *Proc Natl Acad Sci U S A.* 118:e2011226118.
- Huang D, Hu H, Chang L, Liu S, Liang J, Song Y, Wang X, Zhang H, Wei C, Wu Y. 2020. Chinese medicine Bazi Bushen capsule improves lipid metabolism in ovariectomized female ApoE<sup>-/-</sup> mice. *Ann Palliat Med.* 9(3):1073–1083.
- Huang D, Wang X, Zhu Y, Gong J, Liang J, Song Y, Zhang Y, Liu L, Wei C. 2021. Corrigendum: Bazi Bushen capsule alleviates post-menopausal atherosclerosis via GPER1-dependent anti-inflammatory and anti-apoptotic effects. *Front Pharmacol.* 12:774792.
- Jin WN, Shi K, He W, Sun JH, Van Kaer L, Shi FD, Liu Q. 2021. Neuroblast senescence in the aged brain augments natural killer cell cytotoxicity leading to impaired neurogenesis and cognition. *Nat Neurosci.* 24(1):61–73.
- Kaufmann W, Bolon B, Bradley A, Butt M, Czasch S, Garman RH, George C, Gröters S, Krinke G, Little P, et al. 2012. Proliferative and nonproliferative lesions of the rat and mouse central and peripheral nervous systems. *Toxicol Pathol.* 40(4 Suppl.):87S–157S.
- Kim EC, Kim JR. 2019. Senotherapeutics: emerging strategy for healthy aging and age-related disease. *BMB Rep.* 52(1):47–55.
- Kuilman T, Michaloglou C, Mooi WJ, Peeper DS. 2010. The essence of senescence. *Genes Dev.* 24(22):2463–2479.
- Lee J, Kim YS, Kim E, Kim Y, Kim Y. 2020. Curcumin and hesperetin attenuate D-galactose-induced brain senescence *in vitro* and *in vivo*. *Nutr Res Pract.* 14(5):438–452.
- Lei Q, Gao F, Liu T, Ren W, Chen L, Cao Y, Chen W, Guo S, Zhang Q, Chen W, et al. 2021. Extracellular vesicles deposit PCNA to rejuvenate aged bone marrow-derived mesenchymal stem cells and slow age-related degeneration. *Sci Transl Med.* 13:eaz8697.
- Leng F, Edison P. 2021. Neuroinflammation and microglial activation in Alzheimer disease: where do we go from here? *Nat Rev Neurol.* 17(3):157–172.
- Levin O, Fujiyama H, Boisgontier MP, Swinnen SP, Summers JJ. 2014. Aging and motor inhibition: a converging perspective provided by brain stimulation and imaging approaches. *Neurosci Biobehav Rev.* 43:100–117.
- Li L, Chen B, An T, Zhang H, Xia B, Li R, Zhu R, Tian Y, Wang L, Zhao D, et al. 2021. BaZiBuShen alleviates altered testicular morphology and spermatogenesis and modulates Sirt6/P53 and Sirt6/NF- $\kappa$ B pathways in aging mice induced by D-galactose and NaNO<sub>2</sub>. *J Ethnopharmacol.* 271:113810.
- Li L, Zhang H, Chen B, Xia B, Zhu R, Liu Y, Dai X, Ye Z, Zhao D, Mo F, et al. 2022. BaZiBuShen alleviates cognitive deficits and regulates Sirt6/NRF2/HO-1 and Sirt6/P53-PGC-1 $\alpha$ -TERT signaling pathways in aging mice. *J Ethnopharmacol.* 282:114653.
- Long F, Yang H, Xu Y, Hao H, Li P. 2015. A strategy for the identification of combinatorial bioactive compounds contributing to the holistic effect of herbal medicines. *Sci Rep.* 5(1):1–11.
- Magee JC, Grienberger C. 2020. Synaptic plasticity forms and functions. *Annu Rev Neurosci.* 43:95–117.
- Mattson MP, Arumugam TV. 2018. Hallmarks of brain aging: adaptive and pathological modification by metabolic states. *Cell Metab.* 27(6):1176–1199.
- Miguel-Hidalgo JJ, Whittom A, Villarreal A, Soni M, Meshram A, Pickett JC, Rajkowska G, Stockmeier CA. 2014. Apoptosis-related proteins and proliferation markers in the orbitofrontal cortex in major depressive disorder. *J Affect Disord.* 158:62–70.
- Ringland C, Schweig JE, Eisenbaum M, Paris D, Ait-Ghezala G, Mullan M, Crawford F, Abdullah L, Bachmeier C. 2021. MMP9 modulation improves specific neurobehavioral deficits in a mouse model of Alzheimer's disease. *BMC Neurosci.* 22(1):39.
- Rothschild G, Eban E, Frank LM. 2017. A cortical-hippocampal-cortical loop of information processing during memory consolidation. *Nat Neurosci.* 20(2):251–259.
- Saez-Atienzar S, Masliah E. 2020. Cellular senescence and Alzheimer disease: the egg and the chicken scenario. *Nat Rev Neurosci.* 21(8):433–444.
- Singh S, Singh AK, Garg G, Rizvi SI. 2018. Fisetin as a caloric restriction mimetic protects rat brain against aging induced oxidative stress, apoptosis and neurodegeneration. *Life Sci.* 193:171–179.
- Soreq L, Rose J, Soreq E, Hardy J, Trabzuni D, Cookson MR, Smith C, Ryten M, Patani R, Ule J, et al. 2017. Major shifts in glial regional identity are a transcriptional hallmark of human brain aging. *Cell Rep.* 18(2):557–570.
- Sun K, Yang P, Zhao R, Bai Y, Guo Z. 2018. Matrine attenuates D-galactose-induced aging-related behavior in mice via inhibition of cellular senescence and oxidative stress. *Oxid Med Cell Longev.* 2018:7108604.
- Sun K, Sun Y, Li H, Han D, Bai Y, Zhao R, Guo Z. 2020. Anti-ageing effect of *Physalis alkekengi* ethyl acetate layer on a D-galactose-induced mouse model through the reduction of cellular senescence and oxidative stress. *Int J Mol Sci.* 21(5):1836.
- Tewari D, Stankiewicz AM, Mocan A, Sah AN, Tzvetkov NT, Humniecki L, Horbańczuk JO, Atanasov AG. 2018. Ethnopharmacological approaches for dementia therapy and significance of natural products and herbal drugs. *Front Aging Neurosci.* 10:3.
- Varbanov H, Dityatev A. 2017. Regulation of extrasynaptic signaling by polysialylated NCAM: impact for synaptic plasticity and cognitive functions. *Mol Cell Neurosci.* 81:12–21.
- Wang C, Cai X, Wang R, Zhai S, Zhang Y, Hu W, Zhang Y, Wang D. 2020. Neuroprotective effects of verbascoide against Alzheimer's disease via the relief of endoplasmic reticulum stress in A $\beta$ -exposed U251 cells and APP/PS1 mice. *J Neuroinflammation.* 17(1):1–16.
- Wang SC. 2014. PCNA: a silent housekeeper or a potential therapeutic target? *Trends Pharmacol Sci.* 35(4):178–186.
- Wang YL, Wu HR, Zhang SS, Xiao HL, Yu J, Ma YY, Zhang YD, Liu Q. 2021. Catalpol ameliorates depressive-like behaviors in CUMS mice via oxidative stress-mediated NLRP3 inflammasome and neuroinflammation. *Transl Psychiatry.* 11(1):1–12.
- Wei BB, Liu MY, Chen ZX, Wei MJ. 2018. Schisandrin ameliorates cognitive impairment and attenuates A $\beta$  deposition in APP/PS1 transgenic mice: involvement of adjusting neurotransmitters and their metabolite changes in the brain. *Acta Pharmacol Sin.* 39(4):616–625.

- Wiera G, Mozrzymas JW. 2021. Extracellular metalloproteinases in the plasticity of excitatory and inhibitory synapses. *Cells*. 10(8):2055.
- Yan Y, Kong L, Xia Y, Liang W, Wang L, Song J, Yao Y, Lin Y, Yang J. 2018. Osthole promotes endogenous neural stem cell proliferation and improved neurological function through Notch signaling pathway in mice acute mechanical brain injury. *Brain Behav Immun*. 67:118–129.
- Yang J, Wang T, Jin X, Wang G, Zhao F, Jin Y. 2021. Roles of crosstalk between astrocytes and microglia in triggering neuroinflammation and brain edema formation in 1,2-dichloroethane-intoxicated mice. *Cells*. 10(10):2647.
- Yavas E, Gonzalez S, Fanselow MS. 2019. Interactions between the hippocampus, prefrontal cortex, and amygdala support complex learning and memory. *F1000Res*. 8:1292.
- Yousefzadeh MJ, Zhu Y, McGowan SJ, Angelini L, Fuhrmann-Stroissnigg H, Xu M, Ling YY, Melos KI, Pirtskhalava T, Inman CL, et al. 2018. Fisetin is a senotherapeutic that extends health and lifespan. *EBioMedicine*. 36:18–28.
- Zeng F, Wu Y, Li X, Ge X, Guo Q, Lou X, Cao Z, Hu B, Long N, Mao Y, et al. 2018. Custom-made ceria nanoparticles show a neuroprotective effect by modulating phenotypic polarization of the microglia. *Angew Chem Int Ed Engl*. 57(20):5808–5812.
- Zhang B, Lian W, Zhao J, Wang Z, Liu A, Du G. 2021. DL0410 alleviates memory impairment in D-galactose-induced aging rats by suppressing neuroinflammation via the TLR4/MyD88/NF- $\kappa$ B pathway. *Oxid Med Cell Longev*. 2021:6521146.
- Zhang P, Kishimoto Y, Grammatikakis I, Gottimukkala K, Cutler RG, Zhang S, Abdelmohsen K, Bohr VA, Misra Sen J, Gorospe M, et al. 2019. Senolytic therapy alleviates A $\beta$ -associated oligodendrocyte progenitor cell senescence and cognitive deficits in an Alzheimer's disease model. *Nat Neurosci*. 22(5):719–728.
- Zhu Y, Tchkonja T, Pirtskhalava T, Gower AC, Ding H, Giorgadze N, Palmer AK, Ikeno Y, Hubbard GB, Lenburg M, et al. 2015. The Achilles' heel of senescent cells: from transcriptome to senolytic drugs. *Aging Cell*. 14(4):644–658.